Front. Mater. Sci. 2016, 10(4): 413–421
DOI 10.1007/s11706-016-0355-7

RESEARCH ARTICLE

Electrical properties and thermal sensitivity of Ti/Y modified CuO-based ceramic thermistors

Bao YANG[1], Hong ZHANG[1,2], Jia GUO[1], Ya LIU[1], and Zhicheng LI (✉)[1,2]

1 School of Materials Science and Engineering, Central South University, Changsha 410083, China
2 State Key Laboratory of Powder Metallurgy, Central South University, Changsha 410083, China

ABSTRACT: The Ti/Y modified CuO-based negative temperature coefficient (NTC) thermistors, $Cu_{0.988-2y}Y_{0.008}Ti_yO$ (TYCO; y = 0.01, 0.015, 0.03, 0.05 and 0.07), were synthesized through a wet-chemical method followed by a traditional ceramic sintering technology. The related phase component and electrical properties were investigated. XRD results show that the TYCO ceramics have a monoclinic structure as that of CuO crystal. The TYCO ceramics can be obtained at the sintering temperature 970°C–990°C, and display the typical NTC characteristic. The NTC thermal-sensitive constants of TYCO thermistors can be adjusted from 1112 to 3700 K by changing the amount of Ti in the TYCO ceramics. The analysis of complex impedance spectra revealed that both the bulk effect and grain boundary effect contribute to the electrical behavior and the NTC effect. Both the band conduction and electron-hopping models are proposed for the conduction mechanisms in the TYCO thermistors.

KEYWORDS: CuO; TiO_2 substitution; electrical property; negative temperature coefficient; conduction mechanism

Contents

Received July 1, 2016; accepted August 25, 2016

E-mail: zhchli@csu.edu.cn

1 Introduction

Negative temperature coefficient (NTC) thermistors, whose resistances decrease with temperature increasing, have been received considerable attention, and are increasingly applied in automotive, house appliances, and aerospace as elements for suppression of in-rush current, temperature measurements and controlling, etc. Traditional NTC ceramic thermistors always contain transition-metal compounds with spinel structure such as Mn–Ni–O, Ni–Cu–Mn–O and Ni–Mn–Co–O systems, etc. [1–3]. However, the existence of the structural relaxation in those compounds leads to property degradation such as aging, and limits their applications at elevated temperatures ($>$ 300°C) [4]. Much work have reported to improve the electrical properties and ageing resistance of the thermistors with cation doping and microstructure modification [5–7].

In the spinel manganite ceramics, the conduction is generally believed to propagate by an electron hopping mechanism taking place between the Mn^{3+} and Mn^{4+} cations locating on the octahedral sites [8–9]. The exact oxidation states of the Mn cations in the spinel structure obviously depend on the temperature and oxygen partial pressure during sintering, so those ceramics typically exhibit a considerably different in resistivity for a minor change of oxygen partial pressure during sintering or annealing [10–11]. The controllable resistivity, suitable thermal-sensitive constant B, high stability and good accuracy of a NTC thermistor are always required for the real applications. Therefore, to develop new types of NTC thermistors should be of importance and interesting, and attracted much attention in the past years [12–17]. Meanwhile, the NTC thermistors based on single oxide semiconductor, e.g., SnO_2, have obvious merits such as adjustable resistivity by semiconduction doping, suitable thermal-sensitive constant by element substitution, high stability and low cost, etc. [17–19].

Copper oxide, CuO, one of the transition-metal oxides, is a semiconductor with the band gap of about 1.4 eV [20]. Due to low cost, abundant resources and non-toxic feature, CuO becomes potential applications in promising electrode materials for supercapacitors [21] and lithium ion batteries [22]. At the same time, CuO has also been widely used in application such as magnetic storage materials, solar cells, sensors and catalysts, etc. [23–27]. As reported in our previous work [28], CuO-based ceramics can also exhibit excellent NTC characteristics and good reliability in a wide temperature range. In the present work, Y-doped CuO (denoted as YCO) ceramics substituted by various contents of TiO_2 were prepared, the related electrical conductivity, reliability and thermal sensitivity of resistivity were investigated. The results show that the TiO_2-substituted YCO ceramics show the typical NTC behavior and can be obtained at low sintering temperature (lower than 1000°C) which is suitable for the fabrication technology of low-temperature co-sintered ceramics (LTCC). Complex impedance spectra were well-established to investigate the electrical properties of the YCO-based materials.

2 Material and methods

The Y-doped CuO (YCO) powders were prepared by using a wet chemical synthesis method that was polymerized with polyvinyl alcohol (PVA). For the $x = 0.008$ ceramic in the nominal formula of $Cu_{1-3x/2}Y_xO$ ($0.005 \leqslant x \leqslant 0.08$) system has the smallest room-temperature resistivity, the $Cu_{0.988}Y_{0.008}O$ powders, calcined at 830°C for 6 h, were selected for the Ti-substitution study here. A suitable stoichiometry of tetra-n-butyl titanate (TBT, > 99.5%), copper hydroxide ($Cu(OH)_2$, > 95.0%) and yttrium oxide (Y_2O_3, > 99.9%) were weighed, respectively, according to the nominal formula of $Cu_{0.988-2y}Y_{0.008}Ti_yO$ (TYCO, y = 0.01, 0.015, 0.03, 0.05 and 0.07). Appropriate quantity of PVA was added into the solution. The mixed solution was heated with stirring and dried to get the precursor. The precursor was calcined at 830°C for 6 h in air to obtain the TYCO powder. The calcined powder was granulated and pressed into pellets of 12 mm diameter and about 3 mm thickness. The green pellets were subsequently sintered at an optimized temperature 970°C–990°C for 6 h in air. For the investigation of electrical properties, both the surface of the sintered ceramics were polished, coated with silver paste and heated at 600°C for 5 min to make electrodes.

The phase analysis were carried out using X-ray diffraction (XRD, Rigaku D/max 2500, Japan) technique with Cu Kα radiation and $\lambda = 1.54056$ Å in a wide range of Bragg's angles 2θ from 20° to 80° at the scanning rate of 8(°)/min. For the microstructure observation by scanning electron microscope (SEM, FEI Quanta 200), the sintered pellets were broken into pieces, and the fracture surface morphology was observed.

The temperature dependence of resistance (R–T) of each ceramic was tested using a resistance–temperature measurement system (ZWX-C, China) in the direct current (DC) condition, in the temperature range of 25°C–300°C. Alternating current (AC) impedance measurements were carried out by an electrochemical measurement system (Gamry Reference 600, USA) with the frequency ranged from 1 Hz to 1 MHz, at various temperatures.

3 Results and discussion

3.1 Phase and microstructure

The XRD patterns of the as-sintered ceramics of pure CuO, and TYCO (y = 0, 0.03, 0.07) are shown in Fig. 1(a). By being analyzed with a Jade 6.0 + pdf2003 program, all of the ceramics have a monoclinic crystalline structure with the space group of $C2/c$ as that of pure CuO, referred by the powder diffraction file (PDF) no. 80-1917. The lattice parameters of TYCO ceramics were determined to be: a_1 = 0.4672 nm, b_1 = 0.3417 nm, c_1 = 0.5118 nm, β_1 = 99.45° for $y = 0$; a_2 = 0.4751 nm, b_2 = 0.3476 nm, c_2 = 0.5180 nm,

$\beta_2 = 99.57°$ for $y = 0.03$; and $a_3 = 0.4724$ nm, $b_3 = 0.3454$ nm, $c_3 = 0.5174$ nm, $\beta = 99.51°$ for $y = 0.07$. The lattice parameters are slightly different from the ones of the pure CuO ($a = 0.4665$ nm, $b = 0.3413$ nm, $c = 0.5112$ nm, $\beta = 99.42°$). It suggests that Y^{3+} and Ti^{4+} ions have substituted into the lattice of CuO, and the slight changes of the lattice parameters should result from the different ionic radii of the dopants. The Y^{3+} ion (0.101 nm) is larger than Cu^{2+} ion (0.073 nm), leading to a slightly larger lattice. On the other hand, Ti^{4+} ion (0.06 nm) is smaller than Cu^{2+} ion [29], the substitution of Ti^{4+} ions into the lattice sites might cause the slightly lattice reduction.

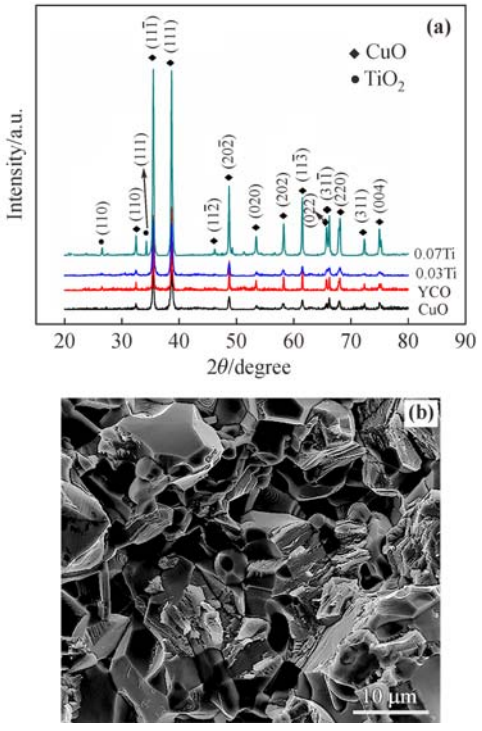

Fig. 1 Phase and microstructure of the as-sintered TYCO ceramics: **(a)** XRD patterns of CuO, $Cu_{0.988}Y_{0.008}O$ (CYO), $Cu_{0.988-2y}Y_{0.008}Ti_yO$ for $y = 0.03$ (0.03Ti) and $y = 0.07$ (0.07Ti); **(b)** SEM image of the as-sintered $Cu_{0.988-2y}Y_{0.008}Ti_yO$ ($y = 0.05$) ceramic.

Y^{3+} ion substitutes into the CuO lattice and occupies the Cu-lattice site, around which the weakly bound electron occurs as described as Eq. (1):

$$Y_2O_3 \xrightarrow{CuO} 2Y_{Cu}^{\cdot} + 2O_O + \frac{1}{2}O_2 + 2e' \qquad (1)$$

The weakly bound electrons locate at the donor level and are easily transport to the conduction level. As a result, the Y^{3+} ion substitution enhances the conductivity. This is the generally as-called band conduction contribution. The Ti^{4+} substitution might also occur weakly bound electrons (2 electrons for a Ti^{4+} substitution) which are similar as that taken place by the Y^{3+} substitution. For an optima conductivity of a semiconductor, there should be an appropriate quantity of weakly bound electrons, beyond which the electron accumulation may occur and hinder the conductivity. This will be further discussed in the next section.

On the other hand, for the differences of radii and valences between Cu^{2+} and Ti^{4+} ions, the introduction of Ti^{4+} ions in the YCO will increase the lattice distortion and there should be a limited solid solubility for Ti^{4+} in the YCO. As the Ti^{4+} concentration increases, e.g., $y = 0.07$, extra diffraction peaks at 2θ of 32.5° and 34.5° can be detected, and were determined to be the crystalline TiO_2. The electron accumulation, lattice distortion and existence of impurity hinder the transport ability and increase the transport energy of the charge carriers, and then the resistivity and conduction activation energy of the TYCO ceramics might increase.

SEM observations of the fracture surface in the as-sintered TYCO ($y = 0.05$) ceramics is illustrated in Fig. 1(b). The nature of the microstructure of TYCO sample shows that the grains densely packed with almost uniform distribution and has low porosity.

3.2 Resistivity–temperature characteristic

Figure 2(a) shows the temperature dependence of resistivity of the TYCO ceramics with different Ti-concentrations. The resistivity values were derived from the measured resistances R according to Eq. (2):

$$\rho = R\frac{\pi r^2}{h} \qquad (2)$$

where, ρ is resistivity, h and r are thickness and radius of each pellet, respectively. It indicates a nearly linear dependence of logarithm of resistivity with reciprocal of absolute temperature over a wide temperature, suggesting a typical NTC behavior of the TYCO ceramics. The relationship between resistivity ($\ln\rho$) and temperature ($10^3/T$) can almost follow Eq. (3):

$$\rho = A\exp\left(\frac{E_a}{kT}\right) = A\exp\left(\frac{B}{T}\right) \qquad (3)$$

where, ρ is the resistivity at temperature T (in Kelvin), A is a constant related to the material characteristic, k is the Boltzmann constant, E_a is the activation energy of conduction, and B is the NTC thermal-sensitive constant

which can be obtained according to Eq. (4):

$$B_{25/85} = \frac{\ln(\rho_{25}/\rho_{85})}{1/T_{25} - 1/T_{85}} \quad (4)$$

where, ρ_{25} and ρ_{85} are the resistivity values at 25°C and 85°C, respectively.

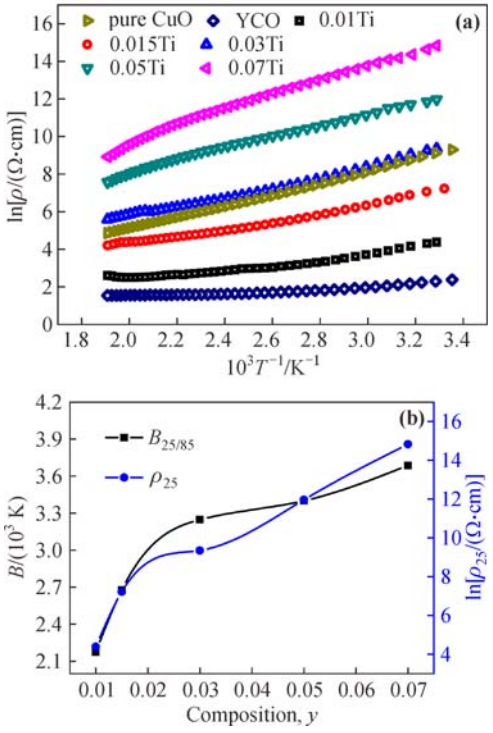

Fig. 2 Electrical properties of TYCO ceramics with various Ti contents: **(a)** resistivity–temperature plots comparing with the ones of pure CuO and YCO; **(b)** TiO_2-concentration dependence of ρ_{25} and $B_{25/85}$.

The additive amount of TiO_2 dependence of ρ_{25} and $B_{25/85}$ of the TYCO ceramics are shown in Fig. 2(b). The values of ρ_{25} are from 80 to 2.75×10^6 Ω·cm when the additive amounts of TiO_2 are 0, 0.01, 0.015, 0.03, 0.05 and 0.07, respectively. The values of thermal-sensitive constants $B_{25/85}$ range from 1112 to 3700 K and are closely dependent of the content of TiO_2. The substitution of Ti^{4+} leads to the increase of the room-temperature resistivity of the YCO ceramics. The substitution of Ti^{4+} ions in the YCO lattice resulted in the lattice distortion and changed the local energy-level status. Meanwhile, the distorted regions act as the scattering center for the charge carrier transport. The mobility of charge carriers decreases, resulting in a rise in the resistance of TYCO ceramics. At the same time, as discussed in Fig. 1, the Ti^{4+} substitution might also produce the weakly bound electrons (2 electrons for a Ti^{4+} substitution) similar as that taken place by the Y^{3+} substitution, but there should be an appropriate quantity of weakly bound electrons in a crystal, the excessive substitution will lead the electron accumulation and hinder the conductivity. On the other hand, the higher amount of TiO_2 could also act as impurity existing at the grain boundaries and increase the resistivity of the ceramics. As the result, the activation energy of conduction (E_a) may increase with the increasing in the substitution of Ti^{4+}, resulting in the increasing of the $B_{25/85}$ of TYCO ceramics.

3.3 Complex impedance analysis

The electrical behavior of an electroceramic is widely characterized by using AC electrochemistry impedance spectroscopy (EIS). Generally, the impedance $Z(\omega)$ is plotted in the Cole-Cole type as Eq. (5):

$$Z(\omega) = Z' + jZ'' \quad (5)$$

where, ω is the angular frequency ($\omega = 2\pi f$), Z' and Z'' are the real and imaginary components of the impedance, respectively, $\sqrt{j} = -1$ is the imaginary factor. Figure 3 shows the Cole-Cole plots of EIS of a TYCO ceramic (y = 0.07) measured at various temperatures. The plots consist of one arc or semicircle, however, it was failed to fit the data with an equivalent circuit related one arc, and are well fitted by the one with a two-parallel RCQ circuits connected in series (see inset in Fig. 3(b)), where, R_g and R_{gb} represent the resistances from the grain effect and grain-boundary effect, respectively; C_g and C_{gb} are the grain capacitance and grain-boundary capacitance, and CPE_g and CPE_{gb} are the constant phase elements (Q) for the effects caused by non-uniform interior structure or some other uncertain defects in grain and grain boundary, respectively. As seen in Fig. 3, the fitted curves are in accordance with the measured data, revealing that the electrical response is composed of two arcs in each impedance spectrum, one from the grain effect and the other is grain-boundary effect. The arcs indicate the departure from the ideal Debye behavior of relaxation phenomenon in the material. The fitted R_g, C_g, R_{gb} and C_{gb} at various temperatures are shown in Table 1. It is clear that both R_g and R_{gb} decrease with rise in temperature and have the typical NTC characteristic. At each measurement temperature, R_g is always higher than R_{gb}.

Figure 4 shows the variation of Z' as a function of frequency for the TYCO (y = 0.07) ceramic at different temperatures. They exhibit that the Z', at each temperature, is larger in the lower frequency region and then becomes a

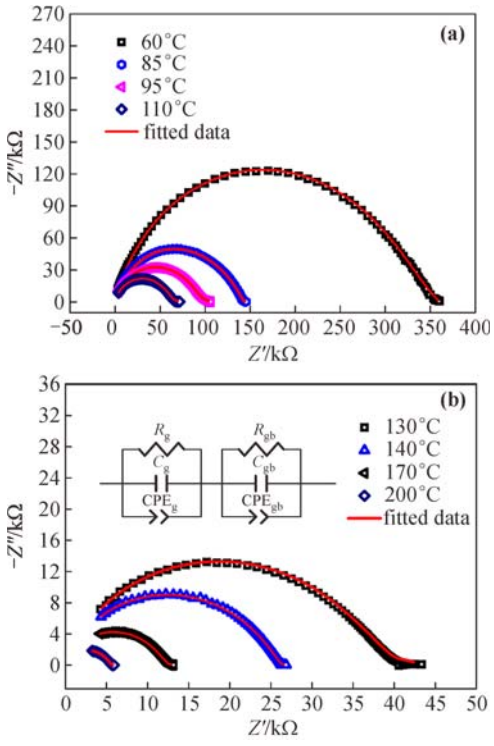

Fig. 3 Nyquist plots of $Cu_{0.988-2y}Y_{0.008}Ti_yO$ ($y = 0.07$) ceramic recorded at various temperatures: **(a)** from 60°C to 110°C; **(b)** from 130°C to 200°C (the inset equivalent circuit used to fit the plots).

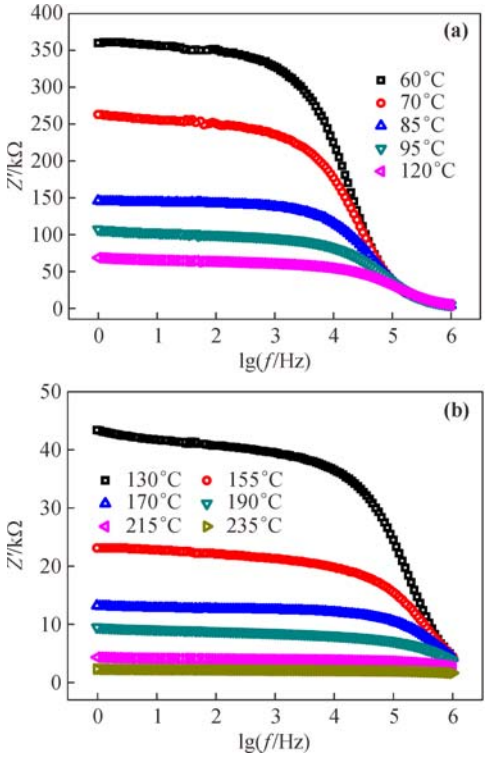

Fig. 4 Variation of real part impedance (Z') with frequency of $Cu_{0.988-2y}Y_{0.008}Ti_yO$ ($y = 0.07$) ceramic at different temperatures: **(a)** from 60°C to 120°C; **(b)** from 130°C to 235°C.

Table 1 The values of resistance and capacitance fitted by an equivalent circuit for a TYCO ceramic ($y = 0.07$) at various temperatures

Temperature /°C	R_{gb} /kΩ	C_{gb} /nF	R_g /kΩ	C_g /pF
60	66.55	0.178	295.6	17.51
85	37.98	0.727	113	5.85
95	16.15	0.105	90.59	11.64
110	12.25	2.2	59.64	2.62
130	6.324	5.3	37.22	2.695
140	1.824	0.852	25.37	10.33
170	1.362	23.89	12.1	5.985
200	0.442	46.55	5.557	7.029

monotonous decrease with the frequency rise. The Z' also shows a decreasing trend with temperature rise in the low frequency region, but tends to merge with the low temperature data in the high-frequency region, suggesting the typical NTC characteristic of the TYCO ceramics. Larger Z' values at lower frequency and temperature indicated larger effects of polarization. In the higher frequency region, all of the curves merge at a low value of Z', which may be due to a possible release of space charge [30].

Figure 5 shows the frequency dependence of the imaginary part (Z'') of impedance of a TYCO ceramic ($y = 0.07$) at different temperatures. The plots show that the Z'' magnitude decreases gradually and the maximum peak (Z''_{max}) shifts towards the higher frequency region when the temperature increases, and the peak broadening becomes more asymmetrical. These should result from the presence of electrical relaxation phenomenon, and are clear proof of a temperature-dependent electrical relaxation process [31]. The peak shifting also suggests that the relaxation time decreases with temperature increasing. The relaxing process should be due to the presence of the immobile electrons at low temperatures and defects at high temperatures [7,32].

In a relaxation system, the relaxation time (τ) can be calculated from Z'' versus lg$f$ plots according to the relationship in Eq. (6):

$$\tau = \frac{1}{\omega} = \frac{1}{2\pi f_{max}} \tag{6}$$

where, f_{max} is the relaxation frequency. The variation of τ as a function of temperature is illustrated in the Fig. 6. It shows that the τ decreases with the temperature rises, suggesting the typical temperature-dependent electrical

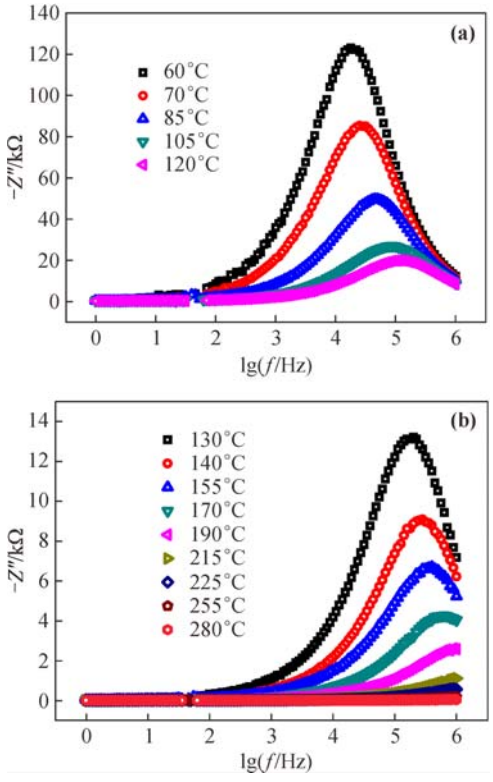

Fig. 5 Frequency dependence of imaginary part impedance (Z'') of $Cu_{0.988-2y}Y_{0.008}Ti_yO$ (y = 0.07) ceramic at different temperatures: **(a)** from 60°C to 120°C; **(b)** from 130°C to 280°C.

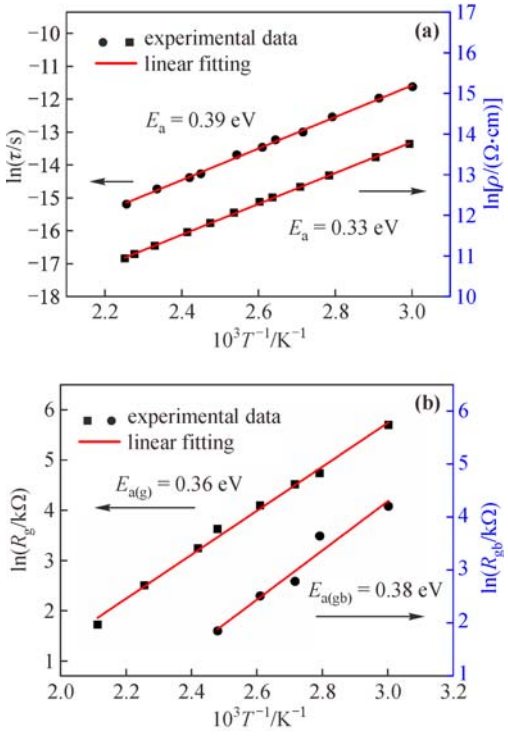

Fig. 6 Comparison of some physical properties of a $Cu_{0.988-2y}Y_{0.008}Ti_yO$ (y = 0.07) ceramic at different temperatures: **(a)** relaxation time and resistivity; **(b)** resistances of grain effect and grain boundary effect.

relaxation phenomena in the TYCO ceramics due to the migration of immobile species. The activation energy (E_a) of the TYCO ceramic can be calculated from the Arrhenius relation Eq. (7):

$$\tau = \tau_0 \exp\left(-\frac{E_a}{kT}\right) \tag{7}$$

where, τ_0 is the pre-exponential factor, k is the Boltzmann constant and T is the absolute temperature. Figure 6(a) shows the variation of relaxation time and resistivity with the temperature ($10^3/T$). The activation energies calculated by the temperature dependence of resistivity based on Eq. (3) (i.e. 0.33 eV) and by the relaxation time variation according to Eqs. (6) and (7) (i.e. 0.39 eV) have similar value. These indicate that the relaxation and conductivity processes possibly result from the same type of charge carriers. Meanwhile, the activation energy of R_g (0.36 eV) matches with the one of R_{gb} (0.38 eV) delivered from Fig. 6(b). It also suggests that the electrical behavior of the TYCO ceramics should result from both the grain effect and grain boundary effect.

3.4 Complex modulus analysis

The complex electric modulus $M(\omega)$ can be calculated from the complex impedance data by using Eq. (8):

$$M(\omega) = M' + \mathrm{j}M'' = \mathrm{j}\omega C_0 Z(\omega) \tag{8}$$

where, M' and M'' are real and imaginary components of the modulus, respectively, $M' = \omega C_0 Z''$ and $M'' = \omega C_0 Z'$, C_0 is geometrical capacitance which is $\varepsilon_0 A/t$, ε_0 is vacuum permittivity, A is the area of the electrode surface and t is the sample thickness. Figure 7(a) shows the complex electric modulus spectrum (M' versus M'') of a TYCO ceramic (y = 0.07) at various temperatures. The pattern is characterized by the presence of the asymmetric semicircular arcs at different temperatures such that they appear to be overlapping for all the temperatures. This may be attributed to the presence of electrical relaxation phenomena. Figure 7(b) shows the variation of M' over a wide range of frequency at various temperatures. A very low value (nearly zero) of M' is observed in the low frequency region. A continuous dispersion on increasing frequency at all the temperatures, contributed to the conduction phenomena, may be due to short-range mobility of charge

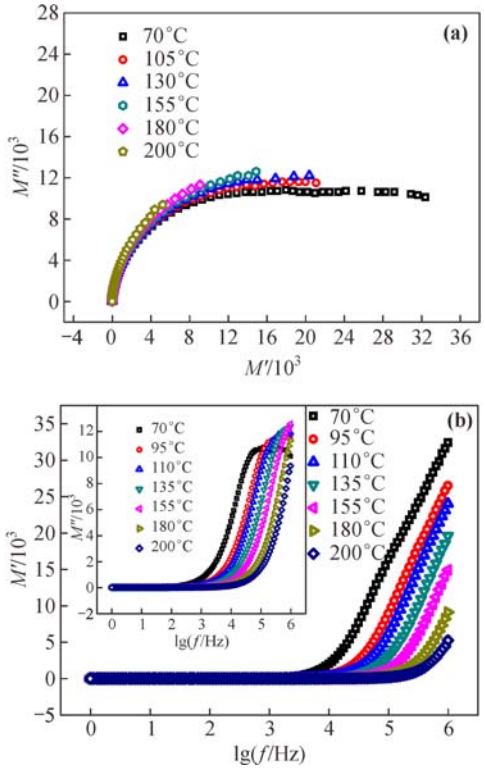

Fig. 7 Characteristic of electric modulus of a $Cu_{0.988-2y}Y_{0.008}Ti_yO$ (y = 0.07) ceramic at different temperatures: **(a)** plots of real part modulus to imaginary one; **(b)** frequency dependence of real part modulus (M'), and the inset is frequency dependence of imaginary part modulus (M'').

carriers [33]. The variation of imaginary part of electric modulus (M'') with frequency at different temperatures is shown in the inset of Fig. 7(b). These exhibit that the imaginary modulus (M''_{max}) peak shifts towards higher relaxation frequencies with rise in temperature, suggesting that the dielectric relaxation is thermally activated process, in which hopping mechanism of charge carriers dominates intrinsically. The asymmetric broadening of the peak indicates the spread of relaxation with different time constant which supports the non-Debye type of relaxation. The magnitude of the peak increases with increasing temperature. The low frequency region of the M'' peak indicates the carriers are mobile over long distance.

On the other hand, the temperature–frequency dependence of electric conductivity can be represented by the Jonscher power law as given by Eq. (9) [34]:

$$\sigma'(\omega) = \sigma'(0) + A\omega^n \tag{9}$$

where, $\sigma'(\omega) = Z'/Z^2$ is the frequency-dependent conductivity of the real part impedance, ω is the angular frequency, $\sigma'(0)$ is the DC conductivity which can be extracted from the value of $\sigma'(\omega)$ when ω tends towards zero, A is the frequency independent constant and n is the power exponent which is frequency independent but temperature and material dependent, and is considered to be hopping conduction when n is less than 1 [34].

Figure 8 shows the double-logarithmic plots of ac conductivity with frequency, $\lg\sigma'(\omega)$ versus $\lg\omega$, of a TYCO ceramic (y = 0.07) at various temperatures. The conductivity $\sigma'(\omega)$, for a certain frequency, increases with the rising in temperature. The conductivities, $\lg\sigma'(\omega)$, keep almost unchangeable in the low frequency region, but they become frequency sensitive at the high-frequency region. The n values estimated by Eq. (9) at various temperatures are always less than 1, and show a decreasing trend with the increasing temperature, indicating the existence of hopping conduction process in the TYCO thermistors. In a transition metal oxide, it is well known that the transition metal might have different ionic valence status, e.g., Cu^+ should exist in the oxide besides Cu^{2+}. The substitution of Y^{3+} and Ti^{4+} into the CuO crystals may enhance the formation of Cu^+ ions to compensate the occurrence of the weakly bound electrons as discussed in Eq. (1). The co-existence of Cu^+ and Cu^{2+} ions provides the temperature-dependent hopping conduction model such as $Cu^{2+} + Cu^+ \leftrightarrow Cu^+ + Cu^{2+}$ in the TYCO ceramic.

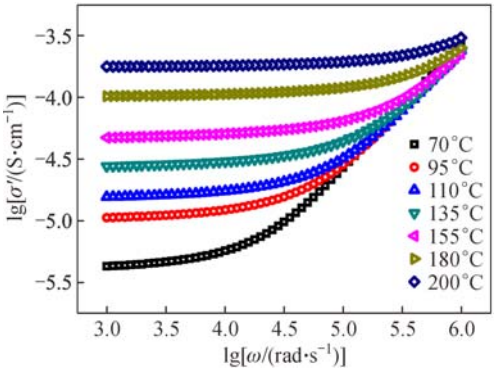

Fig. 8 Double-logarithmic plots ($\lg\sigma'(\omega)$ versus $\lg\omega$) of a $Cu_{0.988-2y}Y_{0.008}Ti_yO$ (y = 0.07) ceramic at various temperatures.

The frequency for the turning point of the conductivity–frequency relationship shifts toward the higher-frequency region when the temperature increases. The frequency independence of AC conductivity in the lower frequency region at each temperature also suggests the long distance movement of charge carriers, i.e., the band conduction model. For the band conduction process, the weakly-bound electrons transport from the donor level to the conduction-bottom level. This process takes place just overcoming a

very small level difference, meaning a small activation energy of conduction and a small NTC thermal-sensitive constant, *B* value. However, in the hopping conduction for the electrons jumping between the ions such as Cu^{+}–Cu^{2+}, the electron needs high enough energy to break away from the Cu^{+} ion and overcomes the lattice barrier. Therefore, the conduction activation energy for hopping process is much higher than that for band conduction. The band conduction and hopping conduction are proposed for the conduction mechanisms in the TYCO thermistors. For the two conduction processes, the band conduction makes higher contribution for the conductivity of TYCO in the low temperature, but the hopping conduction process plays more and more important role in the conductivity when the temperature increases.

4 Conclusions

TiO_2-substituted $Cu_{0.988}Y_{0.008}O$ (TYCO) ceramics were prepared through a wet-chemical synthesis method and sintered at 970°C–990°C. The TYCO ceramics exhibit typical NTC effect over a wide temperature range (25°C–300°C). The room temperature resistivity and thermal-sensitive constant of the TYCO ceramics can be adjusted by changing the content of TiO_2. The electrical behavior of TYCO thermistors resulted from both of the grain effect and grain boundary effect. Long-range mobility of charge carrier (i.e. band conduction) and hopping conduction such as $Cu^{2+} + Cu^{+} \leftrightarrow Cu^{+} + Cu^{2+}$ are proposed for the conduction mechanisms in the TYCO thermistors.

Acknowledgements The authors acknowledge the support of the National Natural Science Foundation of China (Grant No. 51172287) and the Laboratory Research Fund by the State Key Laboratory of Powder Metallurgy, Central South University, China.

References

[1] Feteira A. Negative temperature coefficient resistance (NTCR) ceramic thermistors: an industrial perspective. Journal of the American Ceramic Society, 2009, 92(5): 967–983

[2] Muralidharan M N, Rohini P R, Sunny E K, et al. Effect of Cu and Fe addition on electrical properties of Ni–Mn–Co–O NTC thermistor compositions. Ceramics International, 2012, 38(8): 6481–6486

[3] Golestani-Fard F, Azimi S, Mackenzie K J D. Oxygen evolution during the formation and sintering of nickel–manganese oxide spinels for thermistor applications. Journal of Materials Science, 1987, 22(8): 2847–2851

[4] Feltz A, Pölzl W. Spinel forming ceramics of the system $Fe_xNi_yMn_{3-x-y}O_4$ for high temperature NTC thermistor applications. Journal of the European Ceramic Society, 2000, 20(14): 2353–2366

[5] Fang D L, Chen C S, Winnubst A J A. Preparation and electrical properties of $Fe_xCu_{0.10}Ni_{0.66}Mn_{2.24-x}O_4$ ($0 \leqslant x \leqslant 0.90$) NTC ceramics. Journal of Alloys and Compounds, 2008, 454(1): 286–291

[6] Park K, Han I H. Effect of Al_2O_3 addition on the microstructure and electrical properties of $(Mn_{0.37}Ni_{0.3}Co_{0.33-x}Al_x)O_4$ ($0 \leqslant x \leqslant 0.03$) NTC thermistors. Materials Science and Engineering B, 2005, 119(1): 55–60

[7] Elilarassi R, Chandrasekaran G. Structural, optical and electron paramagnetic resonance studies on Cu-doped ZnO nanoparticles synthesized using a novel auto-combustion method. Frontiers of Materials Science, 2013, 7(2): 196–201

[8] Macklen E D. Electrical conductivity and cation distribution in nickel manganite. Journal of Physics and Chemistry of Solids, 1986, 47(11): 1073–1079

[9] Jung J, Töpfer J, Mürbe J, et al. Microstructure and phase development in $NiMn_2O_4$ spinel ceramics during isothermal sintering. Journal of the European Ceramic Society, 1990, 6(6): 351–359

[10] Fau P, Bonino J P, Demai J J, et al. Thin films of nickel manganese oxide for NTC thermistor applications. Applied Surface Science, 1993, 65: 319–324

[11] Basu A, Brinkman A W, Schmidt R. Effect of oxygen partial pressure on the NTCR characteristics of sputtered $Ni_xMn_{3-x}O_{4+\delta}$ thin films. Journal of the European Ceramic Society, 2004, 24(6): 1247–1250

[12] Xue D, Zhang H, Li Y, et al. Electrical properties of hexagonal $BaTi_{1-x}Fe_xO_{3-\delta}$ (x = 0.1, 0.2, 0.3) ceramics with NTC effect. Journal of Materials Science: Materials in Electronics, 2012, 23 (7): 1306–1312

[13] Nobre M A L, Lanfredi S. Negative temperature coefficient thermistor based on $Bi_3Zn_2Sb_3O_{14}$ ceramic: an oxide semiconductor at high temperature. Applied Physics Letters, 2003, 82(14): 2284–2286

[14] Wang J, Zhang H, Xue D, et al. Electrical properties of hexagonal $BaTi_{0.8}Co_{0.2}O_{3-\delta}$ ceramic with NTC effect. Journal of Physics D: Applied Physics, 2009, 42(23): 235103–235109

[15] Ouyang P, Zhang H, Xue D, et al. NTC characteristic of $SnSb_{0.05}O_2$–$BaTi_{0.8}Fe_{0.2}O_3$ composite materials. Journal of Materials Science: Materials in Electronics, 2013, 24(10): 3932–3939

[16] Upadhyay S, Parkash O, Kumar D. Synthesis, structure and electrical behaviour of lanthanum-doped barium stannate. Journal

of Physics D: Applied Physics, 2004, 37(10): 1483–1491

[17] Zhang J, Zhang H, Yang B, et al. Temperature sensitivity of Fe-substituted SnO_2-based ceramics as negative temperature coefficient thermistors. Journal of Materials Science: Materials in Electronics, 2016, 27(5): 4935–4942

[18] Ouyang P, Zhang H, Zhang Y, et al. Zr-substituted SnO_2-based NTC thermistors with wide application temperature range and high property stability. Journal of Materials Science: Materials in Electronics, 2015, 26(8): 6163–6169

[19] Zhang Y, Wu Y, Zhang H, et al. Characterization of negative temperature coefficient of resistivity in $(Sn_{1-x}Ti_x)_{0.95}Sb_{0.05}O_2$ ($x \leqslant 0.1$) ceramics. Journal of Materials Science: Materials in Electronics, 2014, 25(12): 5552–5559

[20] Ghijsen J, Tjeng L H, van Elp J, et al. Electronic structure of Cu_2O and CuO. Physical Review B: Condensed Matter and Materials Physics, 1988, 38(16): 11322–11330

[21] Dubal D P, Gund G S, Holze R, et al. Mild chemical strategy to grow micro-roses and micro-woolen like arranged CuO nanosheets for high performance supercapacitors. Journal of Power Sources, 2013, 242: 687–698

[22] Chen W, Zhang H, Ma Z, et al. High electrochemical performance and lithiation–delithiation phase evolution in CuO thin films for Li-ion storage. Journal of Materials Chemistry A: Materials for Energy and Sustainability, 2015, 3(27): 14202–14209

[23] Sumikura S, Mori S, Shimizu S, et al. Photoelectrochemical characteristics of cells with dyed and undyed nanoporous p-type semiconductor CuO electrodes. Journal of Photochemistry and Photobiology A: Chemistry, 2008, 194(2–3): 143–147

[24] Anandan S, Wen X, Yang S. Room temperature growth of CuO nanorod arrays on copper and their application as a cathode in dye-sensitized solar cells. Materials Chemistry and Physics, 2005, 93 (1): 35–40

[25] He H, Bourges P, Sidis Y, et al. Magnetic resonant mode in the single-layer high-temperature superconductor $Tl_2Ba_2Cu_{6+\delta}$. Science, 2002, 295(5557): 1045–1047

[26] Ramirez-Ortiz J, Ogura T, Medina-Valtierra J, et al. A catalytic application of Cu_2O and CuO films deposited over fiberglass. Applied Surface Science, 2001, 174(3–4): 177–184

[27] Patil S J, Patil A V, Dighavkar C G, et al. Semiconductor metal oxide compounds based gas sensors: A literature review. Frontiers of Materials Science, 2015, 9(1): 14–37

[28] Yang B, Zhang H, Zhang J, et al. Electrical properties and temperature sensitivity of B-substituted CuO-based ceramics for negative temperature coefficient thermistors. Journal of Materials Science: Materials in Electronics, 2015, 26(12): 10151–10158

[29] Shannon R D. Revised effective ionic radii and systematic studies of interatomic distances in halides and chalcogenides. Acta Crystallographica Section A: Crystal Physics, 1976, 32(5): 751–767

[30] Prasad N V, Prasad G, Bhimasankaram T, et al. Synthesis and electrical properties of $SmBi_5Fe_2Ti_3O_{18}$. Modern Physics Letters B, 1998, 12(10): 371–381

[31] Martínez R, Kumar A, Palai R, et al. Impedance spectroscopy analysis of $Ba_{0.7}Sr_{03}TiO_3/La_{0.7}Sr_{0.3}MnO_3$ heterostructure. Journal of Physics D: Applied Physics, 2011, 44(10): 105302–105310

[32] Azam A, Ahmed A S, Ansari M S, et al. Study of electrical properties of nickel doped SnO_2 ceramic nanoparticles. Journal of Alloys and Compounds, 2010, 506(1): 237–242

[33] Behera B, Nayak P, Choudhary R N P. Structural and impedance properties of $KBa_2V_5O_{15}$ ceramics. Materials Research Bulletin, 2008, 43(2): 401–410

[34] Jonscher A K. The “universal” dielectric response. Nature, 1977, 267(5613): 673–679